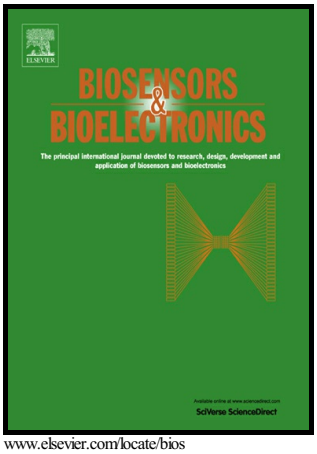

www.elsevier.com/locate/bios

Layer-by-Layer Electrochemical Biosensors Configuring Xanthine Oxidase and Carbon Nanotubes/graphene Complexes for Hypoxanthine and Uric Acid in Human Serum Solutions

Yunpei Si, Jeong Won Park, Sunhee Jung, Geum-Sook Hwang, Eunseo Goh, Hye Jin Lee

PII: S0956-5663(18)30683-3
DOI: https://doi.org/10.1016/j.bios.2018.08.074
Reference: BIOS10738

To appear in: *Biosensors and Bioelectronic*

Received date: 23 June 2018
Revised date: 27 August 2018
Accepted date: 30 August 2018

Cite this article as: Yunpei Si, Jeong Won Park, Sunhee Jung, Geum-Sook Hwang, Eunseo Goh and Hye Jin Lee, Layer-by-Layer Electrochemical Biosensors Configuring Xanthine Oxidase and Carbon Nanotubes/graphene Complexes for Hypoxanthine and Uric Acid in Human Serum Solutions, *Biosensors and Bioelectronic,* https://doi.org/10.1016/j.bios.2018.08.074

Layer-by-Layer Electrochemical Biosensors Configuring Xanthine Oxidase and Carbon Nanotubes/graphene Complexes for Hypoxanthine and Uric Acid in Human Serum Solutions

Yunpei Si[a], Jeong Won Park[b], Sunhee Jung[c,d], Geum-Sook Hwang[c,e], Eunseo Goh[a], Hye Jin Lee[a]*

[a]Department of Chemistry and Green-Nano Materials Research Center, Kyungpook National University, 80 Daehakro, Buk-gu, Daegu-city, 41566, Republic of Korea

[b]SW Contents Research Laboratory, Bio-Medical IT Convergence Research Division, Electronics and Telecommunications Research Institute, 218 Gajeongno, Yuseong-gu, Daejeon, 34129, Republic of Korea

[c]Integrated Metabolomics Research Group, Western Seoul Center, Korea Basic Science Institute, 150, Bugahyeon-ro, Seodaemun-gu, Seoul, 03759, Republic of Korea.

[d]Department of Chemistry, Sungkyunkwan University, 2066, Seobu-ro, Jangan-gu, Suwon-si, Gyeonggi-do, 16419, Republic of Korea.

[e]Department of Chemistry and Nano Science, Ewha Womans University, 52, Ewhayeodae-gil, Seodaemun-gu, Seoul, 03760, Republic of Korea

***Corresponding author:** Postal address: Department of Chemistry and Green-Nano Materials Research Center, Kyungpook National University, 80 Daehakro, Buk-gu, Daegu-city, 41566, Republic of Korea, Tel. + 82 053 950 5336; fax +82 053 950 6330, hyejinlee@knu.ac.kr

Abstract

A selective biosensing platform for the determination of hypoxanthine (Hx) and uric acid (UA) concentrations in both buffer and human serum sample solutions was developed. The biosensor features the layer-by-layer (LbL) self-assembly of negatively charged xanthine oxidase (XOD) and positively charged poly(diallyldimethyl ammonium chloride) (PDDA) wrapped oxidized multi-walled carbon nanotubes and graphene (CNTs-G) complexes (PDDA-CNTs-G) on screen printed carbon electrode (SPCE) surfaces. Catalytic responses of the XOD modified biosensor with the chosen optimum number of layers for LbL assembly on SPCE towards Hx in buffer solutions were first investigated using both cyclic and square wave voltammetries. The peak current at around 0.08 V (vs. Ag/AgCl) associated with the production of UA increased as a function of the Hx concentration due to the surface selective catalytic reaction of XOD and Hx. A linear dynamic range of 5 to 50 μM Hx with a detection limit of 4.40 μM was obtained and the sensor was further applied to the analysis of Hx in normal human serum solutions in addition to myocardial infarction (MI) patient serum sample solutions from a local hospital. Since untreated serum solutions contain a certain amount of UA, a XOD free SPCE biosensor consisted of only PDDA-CNTs-G was also employed to evaluate the native concentration of UA in the serum and further assist the determination of Hx concentration when using the developed LbL biosensor. Our sensing results for the real biological fluidic solutions were finally validated by comparing to those using liquid chromatography-mass spectroscopy (LC-MS).

Graphical Abstract

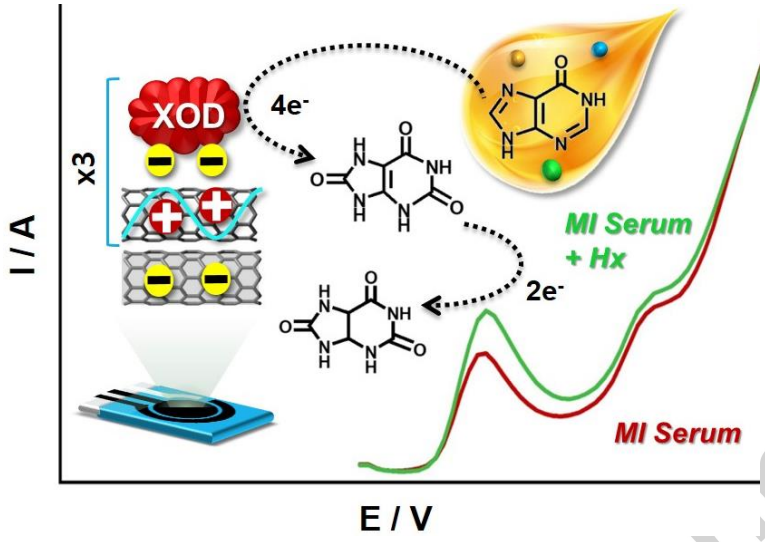

Keywords: Carbon nanotubes-graphene complexes; Hypoxanthine; Uric acid; Layer-by-Layer; Serum; Xanthine Oxidase

1. Introduction

Myocardial ischemia also called cardiac ischemia, which can cause myocardial infarction (MI), heart failure (Minicucci et al., 2011) and also other ischemic heart diseases, is known to be one of the most threatening diseases; for instance, about 32.4 million worldwide MI and stroke patients occur every year (WHO, 2018a), as reported by World Health Organization and a total of 15.2 million deaths occurred in 2016 (WHO, 2018b). It is thus of great significance and necessity to develop a simple and rapid method for the early diagnosis of myocardial ischemia. Over the last decade, numerous efforts have been made on developing different types of diagnostic tools for cardiac ischemia. Electrocardiogram is a widely used clinic diagnosis method for initial screening and detailed information of cardiac ischemia (Ziegler et al., 2016). Alternative approach is the use of biosensing platforms for biomarker proteins which can be correlated to the MI; various sensing platforms have been developed for the key biomarkers including creatine kinase (Sharma et al., 2018), myoglobin (Wang et al., 2015), troponin I and T (Fathil et al., 2015).

Meanwhile, hypoxanthine (Hx), which is a natural metabolite produced during ATP degradation in human beings, is regarded as an important biomarker for the diagnosis of MI. Hx usually exists in healthy human serum around 14 to 38 μM (Caussé et al., 2007) while the elevation of Hx concentration in human blood can be an indicator of MI. For example, the Hx level in blood could be five times higher 60 min after myocardial injury and detectable 15 to 20 min after onset of myocardial ischemia, which is quite earlier and more sensitive than the high specific cardiac biomarker, cardiac troponin T

(cTnT, > 4 h) (Farthing et al., 2015; Lewis et al., 2008; McCann et al., 2008). There have thus been various analysis methodologies reported for Hx concentrations including high-performance liquid chromatography (Cooper et al., 2006; Pleskacova et al., 2016), capillary electrophoresis (Caussé et al., 2007; Domínguez-Álvarez et al., 2017), and hydrophilic interaction ultra-high-performance liquid chromatography-tandem mass spectrometry (Chen et al., 2016). They usually involve a stand-alone sophisticated instrument with a time-consuming procedure and complicated sample pretreatment, in addition to a well-trained operator.

Alternatively, electrochemical biosensors have attracted much attention due to the easy fabrication and rapid detection, as well as good selectivity and sensitivity for point-of-care merits. Extensive efforts have been made on creating electrochemical biosensors for detection of Hx. For example, enzyme-free biosensors for Hx were fabricated on electrode surfaces by modifying with polymer (Ojani et al., 2013; Wang and Tong, 2010), nanoparticles (Lavanya et al., 2016) and carbon material (Luo et al., 2015). The selectivity of biosensors could be improved by incorporating target substrate specific enzymes in the biosensing surface. The electrode modified with xanthine oxidase (XOD) for Hx analysis were developed via measuring oxygen consumption (Haemmerli et al., 1990), uric acid (UA) (Gonzalez et al., 1991) or/and hydrogen peroxide (Torres et al., 2013; Zhang et al., 2012) produced during the enzymatic reaction of XOD and Hx. There have, however, been only a few examples showing the electrochemical sensor applicability to biological fluids such as human serum (Ojani et al., 2013; Wang and Tong, 2010).

The sensitivity of electrochemical biosensors could be improved via the integration of nanomaterials possessing excellent electrical and large surface area properties when configuring electrode surfaces (Wang, 2005). The use of layer-by-layer (LbL) assembly of metallic or carbon nanomaterials and polyelectrolytes could be a superb alternative; two oppositely charged layers consisted of metallic nanoparticles (Barsan and Brett, 2016) or carbon nanomaterial (Lee et al., 2015; Wu et al., 2015), or polyelectrolytes, or biopolymers including proteins, DNA and enzymes can be spontaneously assembled on electrode surface via the electrostatic attraction (Zhao et al., 2006). An example is the use of the LbL assembly of positively charged hexadecyltrimethylammonium coated gold nanocubes and negatively charged poly(sodium 4-styrenesulfonate) and enzyme tyrosinase for the sensitive detection of catechol (Karim et al., 2014).

In this paper, we demonstrated a highly selective electrochemical enzyme biosensor for Hx and UA featuring the LbL assembly of a positively charged poly(diallyldimethyl ammonium chloride) (PDDA) coated carbon nanotubes/graphene complexes (CNTs-G) layer and a negatively charged XOD (pI = 5.3-5.4) (Baş et al., 2014) on SPCEs. Both cyclic and square wave voltammetries were employed to measure current changes associated with the surface site selective electrocatalytic reaction of the substrate Hx and the enzyme XOD assembled on the SPCE to produce UA. As a demonstration, the optimized LbL biosensor was applied to the analysis of Hx concentrations both in normal human and the myocardial infarction patient serum sample solutions from a local hospital. Results were finally compared to those using LC-MS technique.

2. Experimental Section

2.1. Materials

Dopamine hydrochloride (Sigma-Aldrich), glucose monohydrate (Sigma-Aldrich), human serum (Sigma-Aldrich), hydrochloric acid (OCI), hydrogen peroxide (35%) (Junsei), hypoxanthine (Sigma-Aldrich), poly(diallyldimethylammonium chloride) (35 w.t. % in H_2O, Sigma-Aldrich), multi-walled carbon nanotubes (diameter, 20 nm, length 5 μm, Carbon Nano-material Technology), L-ascorbic acid (Sigma-Aldrich), potassium chloride (KCl, Junsei), potassium ferricyanide (III) ($K_3Fe(CN)_6$, Sigma-Aldrich), potassium ferrocyanide (II) ($K_4Fe(CN)_6$, Wako), potassium permanganate (Sigma-Aldrich), sodium hydroxide (NaOH, Sigma-Aldrich), sodium phosphate dibasic (Na_2HPO_4, Merck), sodium phosphate monobasic (NaH_2PO_4, Merck), sulfuric acid (95%, OCI), uric acid (Sigma-Aldrich), xanthine (Sigma-Aldrich), and xanthine oxidase microbial (XOD, lyophilized powder, Sigma-Aldrich) were all used as received. All aqueous solutions were prepared in Millipore-filtered water. Phosphate buffer solution (PB, pH 7.5) was used throughout Hx and UA analysis unless otherwise specified. The xanthine oxidase solution was prepared in 0.1 M PB while the Hx stock solution (0.1 M) was prepared in an acid media consisted of 2:1 ratio of formic acid:H_2O and the desired Hx concentration was prepared by diluting with the PB solution.

2.2. Synthesis of CNTs-G complexes

The CNTs-G was prepared by oxidizing pristine MWCNTs using a modified method reported by Li et al (Li et al., 2012). Briefly, 0.5 g MWCNTs were dispersed in a 40 mL of concentrated H_2SO_4 in an Erlenmeyer flask and stirred at room temperature for 24 h.

A 2.5 g $KMnO_4$ was then added slowly to the suspension while keeping the temperature of the solution lower than 35 ℃. The mixture was stirred for 1 h followed by another 1 h stirring at 65 ℃. Afterward, the reaction was quenched by transferring the flask to an ice water followed by the addition of 5 mL of 30% H_2O_2. The mixture was cooled down and diluted with Millipore filtered water and centrifuged at 10,000 rpm. The supernatant was discarded and the precipitation was washed with 5% HCl solution twice to remove the metal impurities and continuously rinsed with water till the pH of MWCNT solution was around 6. Finally, oxidized MWCNTs forming CNTs-G complexes were dried in the oven at 60 ℃ overnight. Unlike the case of using the mixture of graphene oxide (GO) and CNT to form reduced GO-CNT complexes (Uzunoglu et al., 2018), the exact ratio of the CNTs versus graphene in our CNTs-G complexes was difficult to estimate because only MWCNT was used as a raw material, not the mixture when synthesizing the complexes.

2.3. Fabrication of LbL biosensor

A simplified scheme showing the LbL assembly of XOD and CNTs-G-PDDA on a SPCE is presented in Fig. 1(a). The surface of SPCE was first rinsed with ethanol and distilled water followed by drying it with an air blower, and treated by an oxygen plasma for 30 s at 100 W. This provides a clean and hydrophilic surface for LbL assembly. A 5 µL of 0.5 mg mL^{-1} of CNTs-G prepared in Millipore-filtered water (pH 8, adjusted by 1 M NaOH) was dropped on the oxygen plasma treated working electrode surface then washed with distilled water after air dried. The LbL assembly was then achieved by sequential dropping a 20 µL of 1% PDDA coated CNTs-G (0.5

mg mL^{-1}) prepared in Millipore-filtered water and a 10 µL of 100 U mL^{-1} XOD onto the CNTs-G modified SPCE (see details in Supporting Information). This was repeated for desired layers of LbL on the electrode. Each layer adsorbed on the electrode was incubated for 20 min at 4 ℃ and carefully washed with the PB solution and dried for the next layer assembly. The LbL biosensor was finally stored at 4 ℃ prior to any further experiments. The surface morphology and roughness of the LbL sensor were studied by field emission scanning electron microscope (FE-SEM, SU8220, Hitachi), and confocal laser scanning microscope (CLSM, Carl Zeiss LSM 700).

2.4. Electrochemical Measurements

All electrochemical data including cyclic and square wave voltammetries were obtained using a computer-controlled potentiostat (Autolab PGSTAT128N) operated by the General Purpose Electrochemical system (GPEs) program (version 4.9). The custom-made SPCE is composed of three electrodes, a carbon working electrode with a geometric working area of 28 mm^2, an Ag/AgCl reference and a carbon counter electrode. Prior to any electrochemical measurements, the enzyme modified LbL biosensor immersed in the PB solution was scanned several times to obtain a stable background signal. When a stock solution of Hx or UA was added in the buffer for a desired concentration, the immersed electrode was incubated for 1 min prior to any electrochemical measurements. The real sample analysis was conducted in 15-fold diluted normal human and MI patient serum sample solutions using the LbL biosensor and the other XOD free biosensor. All the electrochemical measurements were repeated at least three times and averaged for data analysis.

2.5. LC-MS Analysis

For quantitative analysis of Hx and UA, ultra-high performance LC/triple quadrupole (TQ) MS analysis was performed on Agilent 1290 Infinity LC and an Agilent 6495 triple quadrupole MS system equipped with an Agilent Jet Stream electrospray ionization source (Agilent Technologies, USA). Details on the LC separation can be found in the supporting information. Prior to the analysis, serum samples were pretreated as follows: a 50 μL of serum sample was used to extract serum metabolites. Chloroform/methanol (2:1, v/v) was added and vigorously mixed. Then, water was added to each sample tube and vortexed. The sample solution was incubated at 4 °C for 10 min and centrifuged. The supernatant was dried in a vacuum concentrator. The extracts were diluted with an acetonitrile/water mixture (2:8, v/v) and transferred to LC vials.

3. Results and Discussion

3.1. Characterization of LbL biosensors

The water dispersibility of CNTs-G complexes is required in order for assembling them evenly on the electrode thus a strong acid treatment was used. As can be seen from Fig. S1 the acid treated CNTs-G complexes were homogeneously dispersed in Millipore-filtered water (Fig. S1b) while the pristine MWCNTs easily aggregated due to the hydrophobic sidewall (Fig. S1a). However, the MWCNTs were shortened and some CNTs-G complexes formed as the outer walls were exfoliated during the harsh oxidation process (see FE-TEM images in Fig. S2). The hydrophilicity and functional

groups of CNTs-G complexes were first confirmed via FT-IR measurements (Fig. S3); the characteristic peaks at 3436 cm^{-1} and a small shoulder peak at around 1714 cm^{-1} attributed to the stretching of -OH and C=O of the carboxylic group, respectively were found for the CNTs-G complexes. The wide peak at 1095 cm^{-1} is because of the epoxy group on the CNTs-G complexes. Whereas the absorption peaks at 3441 and 1628 cm^{-1} corresponding to the stretching of -OH and C=C; the peaks at 2918 and 2850 cm^{-1} due to the stretching of =C-H for the pristine MWCNTs.

To further confirm the surface element composition of CNT-G complexes, X-ray photoelectron spectroscopy (XPS, ULVAC-PHI, Quantera SXM) measurements were performed and the results were also compared to those of using MWCNTs and PDDA-CNTs-G (see Fig 2). The MWCNTs spectra (Fig. 2a, i) showed the typical C1s peak while a clear O1s peak of the CNTs-G (Fig. 2a, ii) appeared. After coating the CNTs-G with PDDA, N1s peak assigned for PDDA was shown. The detailed C1s XPS spectra of MWCNTs also confirmed peaks of C=C (284.4 eV) and C-C (285.5 eV) in addition to the π-π* shake up similar to those of previous reports (Okpalugo et al., 2005; Yang et al., 2011). By contrast, the C1s deconvoluted spectra of CNTs-G illustrated the bonds of C-O-C (286.5 eV) and O-C=O (288.4 eV) alongside the bonds also present in MWCNTs. The existence of C-O-C and O-C=O in CNTs-G is consistent with our FT-IR results shown in Fig. S3. Furthermore, the C-N bonding peak (286.8 eV) corresponding to PDDA in Fig. 2(d) confirmed the functionalization of PDDA on CNTs-G.

Prior to any sensing applications, the surface characteristics of LbL biosensors

featuring XOD and PDDA-CNTs-G complexes were studied using FE-SEM and CLSM. A dense layer of CNTs-G was observed after the LbL assembly on the SPCE electrode surface while the enzyme adsorption was insignificant when using FE-SEM (Fig. 1). The presence of XOD layer was, however, confirmed via the electrochemical catalytic response for Hx to produce the corresponding oxidation peaks assigned to UA. CLSM results also revealed that the presence of LbL resulted in an increase of average roughness depth value of ~14 μm compared to that of the bare SPCE (~10 μm).

Electrode surfaces of bare, CNTs-G modified and LbL SPCE biosensors were characterized in 5 mM $Fe(CN)_6^{3-/4-}$ prepared in 0.1 M KCl solution by cyclic voltammetry with a scan rate of 50 mV s^{-1} (see Fig. S4). Well-defined redox peaks were observed for bare and CNTs-G modified SPCE. After modification with CNTs-G, the peak-to-peak separation potential (ΔE_p) was reduced and the redox peak current increased markedly due to the high conductivity and large surface area of CNTs-G consequently facilitating the electron transfer and current amplification during $Fe(CN)_6^{3-/4-}$ redox process. A decrease of the redox peak current was observed after the LbL self-assembly of oppositely charged layers which could be attributed to the occupation of active sites for $Fe(CN)_6^{3-/4-}$ species by XOD and electrostatic repulsion between the negatively charged enzyme layer and $Fe(CN)_6^{3-/4-}$ species. The electroactive surface area of different electrodes was calculated by using the Randles-Sevcik equation (1) developed for the diffusion controlled reversible reaction (Bard and Faulkner, 2001; Na et al., 2016).

$$i_p = (2.69 \times 10^5) n^{3/2} A C_0 {D_0}^{1/2} v^{1/2} \quad (1)$$

where i_p is the peak current (A), n is the number of electrons participating in the redox reaction, A is the electroactive area (cm^2), v is the scan rate ($V\ s^{-1}$), D_0 is the diffusion coefficient ($cm^2\ s^{-1}$) and C_0 is the concentration of redox species ($mol\ cm^{-3}$) at 25 ℃. The calculated electroactive surface areas of bare SPCE, CNTs-G-SPCE, and LbL biosensor are 4.5×10^{-2} cm^2, 33.6×10^{-2} cm^2, and 24.8×10^{-2} cm^2, respectively. The electroactive surface area of CNTs-G-SPCE was more than 7-fold of bare SPCE and even larger than the geometric surface area (28×10^{-2} cm^2) of the electrode. In case of LbL biosensors, a smaller electroactive surface area was obtained compared with CNTs-G-SPCE as the active sites of CNTs-G for $Fe(CN)_6^{3-/4}$. However, this value is still much higher than the bare SPCE electroactive surface area.

3.2. Electrochemical analysis of UA and Hx

Amperometric measurements utilizing direct oxidation of Hx appeared at a high potential (~ 0.86 V vs. Ag/AgCl) can be often interfered with the direct oxidation of many other compounds including UA, ascorbic acid, and xanthine in addition to water split reaction. The use of enzyme reaction or redox mediator lowering the oxidation potential value of the target can be a great alternative; for instance, a mediator phenazine methosulfate was employed for the catalytic detection of Hx at - 90 mV (vs. Ag/AgCl) by using cyclic voltammetry method even lower than that of UA oxidation to

avoid the interference of UA (Kalimuthu et al., 2012). Our idea of developing Hx sensitive LbL biosensor is based on measuring the current associated with the catalytic reaction of the surface bound XOD with Hx to produce UA following the scheme below.

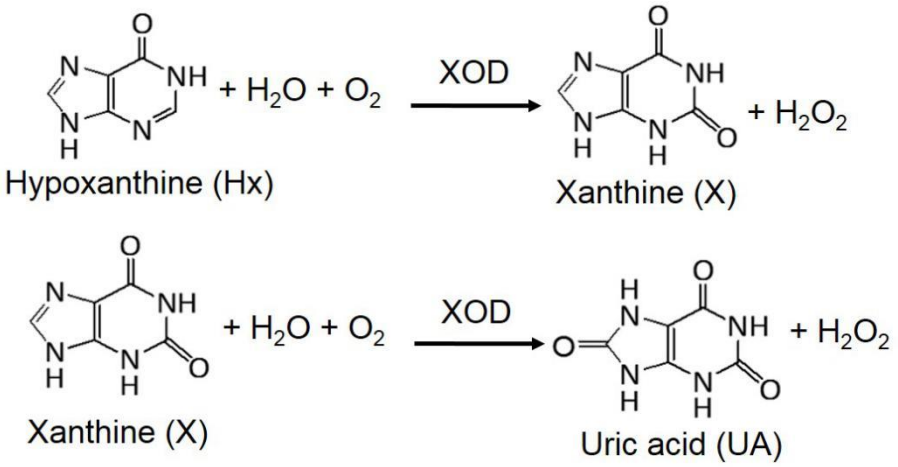

The number of XOD and CNTs-G complexes layers were next characterized via the catalytic reaction of the surface bound XOD with Hx to produce UA following the scheme. When immersing the LbL biosensor in a fixed concentration of 50 μM Hx, the peak at about 0.12 V (vs. Ag/AgCl) appeared. As the number of XOD layer increased up to three, the peak current responsible for UA increased; however the increase of XOD layers to five did not significantly affect the current increment anymore, which probably due to the fact that the dense thick LbL layers could hinder the electron generated by the XOD catalytic reaction moving towards the electrode surface (Fig. S5). Thus three layers of XOD in the LbL biosensor was chosen and used throughout the Hx and UA analysis. Note that there is a slight variation of the peak potential between 0.06 V to 0.16 V for Hx oxidation to produce UA due to minimal uncompensated *iR* drop.

The diffusion controlled Hx reaction with XOD on the (XOD-PDDA-CNTs-G)$_3$-CNTs-G-SPCE LbL biosensor was also investigated using CV with varying scan rates at fixed 30 and 50 µM Hx solution (Fig. S6). The peak current of UA at 0.06 V (vs. Ag/AgCl) due to the oxidation of Hx via XOD increased with respect to the square root of the scan rate following the Randles-Sevcik equation (2) for an irreversible reaction (Na et al., 2016):

$$i_{\mathrm{p}} = (2.99 \times 10^5) n^{3/2} \alpha^{1/2} A C_0 {D_0}^{1/2} v^{1/2} \quad (2)$$

where α is transfer coefficient. This indicates that the observed peak current is due to the diffusion controlled process, not by the adsorption of the catalytic Hx reaction on the enzyme modified electrode.

With the confirmation of diffusion controlled Hx reaction when using the optimized 3 layers of LbL biosensor, Hx and UA analysis was investigated using square wave voltammetric method (SWV) which offers a clear oxidation peak shape, high sensitivity, and fast data acquisition. As can be seen in Fig. 3(a), the oxidation peak current of UA in the absence of Hx at around 0.08 V (vs. Ag/AgCl) showed a linear range of 5-140 µM with a sensitivity of 0.296 µA/µM and a lowest detectable concentration of 2 µM. The Hx quantitation was achieved via measuring the peak oxidation current of UA produced by the catalytic reaction of the substrate Hx and the enzyme XOD in the LbL sensor. The UA peak at around 0.08 V (vs. Ag/AgCl)

increased linearly as a function of the Hx concentration ranging from 5 to 50 µM with a sensitivity of 0.241 µA/µM (R^2=0.994) and a limit of detection of 4.40 µM ($3S_b/m$) Hx on the $(XOD\text{-}PDDA\text{-}CNTs\text{-}G)_3$-CNTs-G-SPCE LbL biosensor (Fig. 3b). For the concentration range above 50-90 µM, a lower sensitivity of 0.124 µA/µM (R^2=0.988) was obtained which often occurs when using the surface sensitive biosensors (Karim et al., 2014; Teymourian et al., 2012; Zhao et al., 2015). Also a peak at 0.86 V assigned for the direct oxidation of Hx increased as the Hx concentration increased, however, as the enzyme reaction processed, the peak decreased. In addition, the percentage of Hx converted to UA via the XOD catalytic reaction was estimated as ~70 % based on the comparison of both calibration plots of direct UA oxidation and UA oxidation resulted from Hx during enzymatic detection (see Fig. 3).

The capability of detecting Hx at a concentration range of 5 to 50 µM is sufficient for the Hx analysis in biological samples particularly for the diluted MI patient samples. Such an LbL sensors performance is attributed to the use of CNTs-G complexes in the PDDA layer. An LbL biosensor assembled only with PDDA instead of using CNTs-G-PDDA with the optimum 3 layers was configured and used for the Hx analysis; a slightly narrower linear range from 10 to 50 µM with a lower sensitivity of 0.166 µA/µM (R^2 = 0.995) were obtained indicating that the played an important role in improving the LbL sensors sensitivity (see Fig. S7 and Table S1).

3.3. Reproducibility, selectivity and stability of LbL biosensors

Prior to biological sample analyses, the reproducibility of LbL biosensors was

investigated by measuring the SWV responses of five different chips prepared independently at the fixed concentration of Hx. The relative standard deviation (RSD) values of 5.88% and 3.16% were obtained for 30 and 50 μM Hx, respectively (Fig. S8). In addition, the storage stability of our LbL biosensors was also measured via storing them at 4 ℃ in PB solution for a certain period and measured the current signal for 50 μM Hx. Around 16% of the LbL sensor activity was lost after a 3-day storage and only half of the activity left after one week which may due to the short life time of XOD (Albelda et al., 2017; Arai et al., 1996).

To ensure the selectivity of our sensor when dealing with the biological sample, interfering effects were investigated for the detection of 20 μM Hx in 15-fold diluted human serum with expected high concentrations of interfering reagents including glucose (Glu 5 mM), ascorbic acid (AA 20 μM), xanthine (X 5 μM), and dopamine (DA 1 μM) (Dungchai et al., 2009; Ghita and Arrigan, 2004; Kangkamano et al., 2017; Ruecha et al., 2014). There was no interference from Glu, and negligible effect from DA while the current for Hx increased 13.7% and 13.9% when AA and X added, respectively (Fig. S9).

3.4. Real sample analysis

The determination of Hx in human biological fluids is essential for the early diagnosis of cardiac ischemia. As a final demonstration, the LbL biosensor was applied to diluted human serum samples including normal human and MI patient serum solutions. Prior to the analysis, any existing (native) UA concentrations in the sample should be taken into account since our Hx quantification relies on quantitating resulting oxidation peak

currents of the enzymatic product, UA. An XOD enzyme free electrochemical sensor was thus used to estimate the oxidation peak solely from the native UA concentration in diluted serum samples; the XOD free sensor for UA concentrations in the buffer solution was characterized and the sensitivity similar to that of the LbL sensor containing the enzyme was confirmed (Fig. S10). Note that there is another XOD substrate, namely xanthine (X), present in the serum which could generate UA affecting in the total UA signal of the serum; however, the oxidation of UA produced from the reaction between XOD and X was not considered since the X concentration in human serum solutions is much lower than that of Hx (Caussé et al., 2007; Cooper et al., 2006).

Considering the limited amount of the patient serum sample and also the detection range of the LbL sensor, the serum samples were diluted 15-fold, with pH 7.5 PB solution. The recovery study of Hx in the normal human samples was performed using a standard addition method in which 10, 15 and 20 μM Hx solution were successively spiked into the samples. SWV analysis for both normal human serum and MI patient serum samples by LbL biosensor are shown in the curve (i), Fig. 4 (a) and (b), respectively showing that the peak at around 0.22 V is regarded as the total oxidation signal of both the UA generated from Hx catalyzed with XOD and the UA originally existing in human serums. The curve (i) in Fig. 4 is the total current signal response from the LbL biosensor whereas the curve (ii) is the signal from the native UA present in the diluted serum solutions when using the XOD free sensor. The current for Hx concentration in the serum solution was determined by subtracting the UA oxidation peak current (ii) from the curve (i) (see calculation details in Supporting Information and Table S2). When 10, 15, 20 μM Hx were individually spiked into the diluted serum samples (Fig. 4

curve iii, iv, and v, respectively), Hx quantitation in the samples can also be achieved by subtracting the total Hx signal from original UA (curve ii). A reasonable correlation of the MI patient sample analysis for Hx using both methods was obtained within the relative error 0.1%. In addition, the recoveries between 91.1 and 101.9% were obtained for Hx determination in diluted normal human serum solutions. Moreover, the UA concentration in the same diluted human serum solution was also estimated. The analysis results are summarized in Table 1 and 2 alongside the comparison results by an LC-MS method.

The discrepancy appeared particularly for diluted healthy normal human serum sample analysis is due to the LbL sensors detection capability; the improvement of the detectability down to sub μM Hx could be achieved via future efforts such as introducing innovative novel nanomaterials for electrode engineering. Nevertheless, it must be mentioned that the acceptable Hx analysis results were obtained in diluted MI patient serum sample by the LbL sensor, which confirms the feasibility of our LbL biosensor for real biological sample analyses. Finally, a summary of our SWV based LbL biosensors performance for Hx detection compared to those of recently published other works using electrochemical methods is shown in Table S3. A reasonable limit of detection with a low micromolar dynamic range is obtained for the Hx detectability of our LbL biosensors alongside real human biological sample applicabilities.

4. Conclusion

A disposable and sensitive electrochemical LbL enzyme biosensor by self-assembly of positively charged layer of PDDA-CNTs-G and negatively charged XOD layer

alternatively on SPCE and a XOD free sensor were developed for the fast and selective determination of Hx and UA in diluted human serum samples. A dynamic range of 5 to 50 μM Hx with a detection limit of 4.40 μM was achieved. Compared with some of recent works in Table S3, our sensing platforms showed a lower detection limit (Albelda et al., 2017) for Hx with a linear dynamic range for the low micromolar Hx concentration (Luo et al., 2015). The CNTs-G complexes were employed in the layers not only for amplifying biosensors signal but also for providing a large surface area for enzyme adsorption. The acceptable detection results and recovery in human and MI patient serum samples indicate a great potential of our sensing platform for the hypoxanthine for clinical diagnosis. The interference from ascorbic acid is one of the challenging issues which will be presented in future studies possibly by engineering sensors surface with new materials to improve the selectivity and sensitivity for Hx.

Acknowledgment

This work was supported by the National Research Council of Science & Technology (NST) grant by the Korea government (MSIP) (No. CAP-12-2-KBSI) and the National Research Foundation (NRF) of Korea funded by the Ministry of Science, ICT, and Future Planning (Grant number: NRF-2016R1A2B4012026).

References

Albelda, J.A.V., Uzunoglu, A., Santos, G.N.C., Stanciu, L.A., 2017. Biosens. Bioelectron. 89(1), 518-524.
Arai, G., Takahashi, S., Yasumori, I., 1996. J. Electroanal. Chem. 410(2), 173-179.
Bard, A.J., Faulkner, L.R., 2001. Electrochemical Methods: Fundamentals and Applications, 2nd Edition, p. 231. John Wiley & Sons, Inc., New York.
Barsan, M.M., Brett, C.M.A., 2016. TrAC, Trends Anal. Chem. 79, 286-296.
Caussé, E., Pradelles, A., Dirat, B., Negre -Salvayre, A., Salvayre, R., Couderc, F., 2007. Electrophoresis 28(3), 381-387.
Chen, J., Hou, W., Han, B., Liu, G., Gong, J., Li, Y., Zhong, D., Liao, Q., Xie, Z., 2016. Anal. Bioanal.

Chem. 408(10), 2527-2542.
Cooper, N., Khosravan, R., Erdmann, C., Fiene, J., Lee, J.W., 2006. J. Chromatogr. B 837(1-2), 1-10.
Domínguez-Álvarez, J., Mateos-Vivas, M., Rodríguez-Gonzalo, E., García-Gómez, D., Bustamante-Rangel, M., Zamarreño, M.-M.D., Carabias-Martínez, R., 2017. TrAC, Trends Anal. Chem. 92, 12-31.
Farthing, D.E., Farthing, C.A., Xi, L., 2015. Exp. Biol. Med. 240(6), 821-831.
Fathil, M.F.M., Arshad, M.K.M., Gopinath, S.C.B., Hashim, U., Adzhri, R., Ayub, R.M., Ruslinda, A.R., Nuzaihan, M.N.M., Azman, A.H., Zaki, M., Tang, T.-H., 2015. Biosens. Bioelectron. 70, 209-220.
Gonzalez, E., Pariente, F., Lorenzo, E., Hernandez, L., 1991. Anal. Chim. Acta 242, 267-273.
Haemmerli, S.D., Suleiman, A.A., Guilbault, G.G., 1990. Anal. Lett. 23(4), 577-588.
Karim, M.N., Lee, J.E., Lee, H.J., 2014. Biosens. Bioelectron. 61, 147-151.
Lavanya, N., Sekar, C., Murugan, R., Ravi, G., 2016. Mater. Sci. Eng., C 65, 278-286.
Lee, T., Min, S.H., Gu, M., Jung, Y.K., Lee, W., Lee, J.U., Seong, D.G., Kim, B.-S., 2015. Chem. Mater. 27(11), 3785-3796.
Lewis, G.D., Wei, R., Liu, E., Yang, E., Shi, X., Martinovic, M., Farrell, L., Asnani, A., Cyrille, M., Ramanathan, A., Shaham, O., Berriz, G., Lowry, P.A., Palacios, I.F., Taşan, M., Roth, F.P., Min, J., Baumgartner, C., Keshishian, H., Addona, T., Mootha, V.K., Rosenzweig, A., Carr, S.A., Fifer, M.A., Sabatine, M.S., Gerszten, R.E., 2008. J. Clin. Invest. 118(10), 3503-3512.
Li, Y., Zhou, W., Wang, H., Xie, L., Liang, Y., Wei, F., Idrobo, J.-C., Pennycook, S.J., Dai, H., 2012. Nat. Nanotechnol. 7(6), 394-400.
Luo, A., Lian, Q., An, Z., Li, Z., Guo, Y., Zhang, D., Xue, Z., Zhou, X., Lu, X., 2015. J. Electroanal. Chem. 756, 22-29.
McCann, C.J., Glover, B.M., Menown, I.B.A., Moore, M.J., McEneny, J., Owens, C.G., Smith, B., Sharpe, P.C., Young, I.S., Adgey, J.A., 2008. Eur. Heart J. 29(23), 2843-2850.
Minicucci, M.F., Azevedo, P.S., Polegato, B.F., Paiva, S.A.R., Zornoff, L.A.M., 2011. Clin. Cardiol. 34(7), 410-414.
Na, Z., Liang, F., Yin, D., Wang, L., 2016. RSC Adv. 6(61), 56399-56405.
Ojani, R., Alinezhad, A., Abedi, Z., 2013. Sens. Actuators, B 188, 621-630.
Okpalugo, T.I.T., Papakonstantinou, P., Murphy, H., McLaughlin, J., Brown, N.M.D., 2005. Carbon 43(1), 153-161.
Pleskacova, A., Brejcha, S., Pacal, L., Kankova, K., Tomandl, J., 2016. Chromatographia 80(4), 529-536.
Sharma, A.K., Pandey, S., Nerthigan, Y., Swaminathan, N., Wu, H.-F., 2018. Anal. Chim. Acta 1024, 161-168.
Teymourian, H., Salimi, A., Hallaj, R., 2012. Biosens. Bioelectron. 33(1), 60-68.
Torres, A.C., Ghica, M.E., Brett, C.M.A., 2013. Anal. Bioanal. Chem. 405(11), 3813-3822.
Uzunoglu, A., Kose, D.A., Kose, K., Gokmese, E., Gokmese, F., 2018. MRS Commun., 1-7.
Wang, J., 2005. Analyst 130(4), 421-426.
Wang, Q., Liu, F., Yang, X., Wang, K., Wang, H., Deng, X., 2015. Biosens. Bioelectron. 64, 161-164.
Wang, Y., Tong, L.-l., 2010. Sens. Actuators, B 150(1), 43-49.
http://www.who.int/cardiovascular_diseases/priorities/secondary_prevention/country/en/index1.html. 2018a (Accessed on 21 June 2018)
http://www.who.int/en/news-room/fact-sheets/detail/the-top-10-causes-of-death. 2018b (Accessed on 21 June 2018)
Wu, B., Hou, S., Miao, Z., Zhang, C., Ji, Y., 2015. Nanomaterials 5(3), 1544-1555.
Yang, S.-Y., Lin, W.-N., Huang, Y.-L., Tien, H.-W., Wang, J.-Y., Ma, C.-C.M., Li, S.-M., Wang, Y.-S., 2011. Carbon 49(3), 793-803.
Zhang, L., Lei, J., Zhang, J., Ding, L., Ju, H., 2012. Analyst 137(13), 3126-3131.
Zhao, H., Ji, X., Wang, B., Wang, N., Li, X., Ni, R., Ren, J., 2015. Biosens. Bioelectron. 65, 23-30.
Zhao, W., Xu, J.-J., Chen, H.-Y., 2006. Electroanalysis 18(18), 1737-1748.
Ziegler, M., Alt, K., Paterson, B.M., Kanellakis, P., Bobik, A., Donnelly, P.S., Hagemeyer, C.E., Peter, K., 2016. Sci. Rep. 6, 38161.

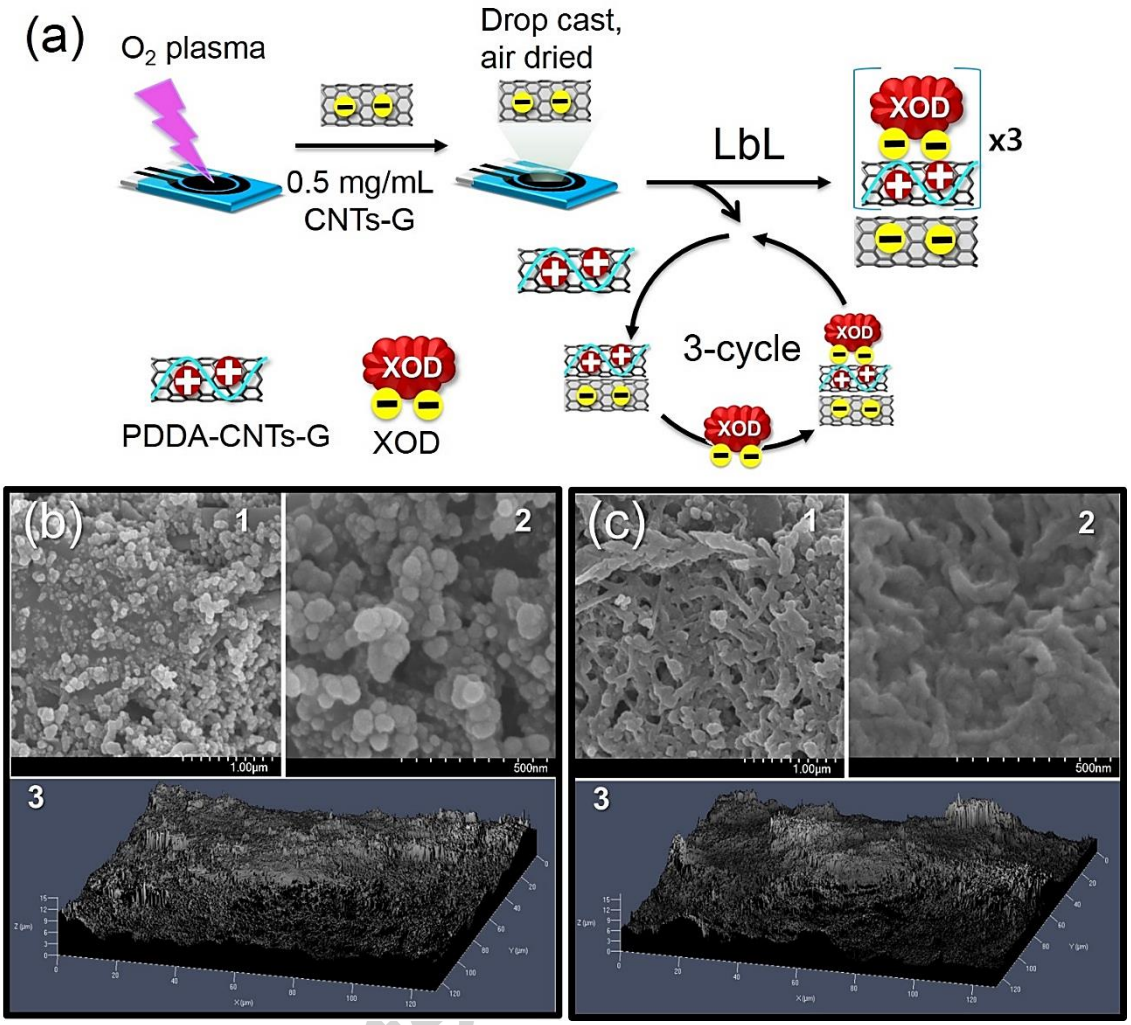

Fig. 1 (a) Schematic showing the fabrication of LbL biosensor on SPCE, (b) (1,2) FE-SEM and (3) CLSM images (500 x magnification, 120 x 120 μm area) of bare SPCE surface; and (c) (1,2) FE-SEM and (3) CLSM images (500 x magnification, 120 x 120 μm area) of LbL biosensor composed of $(XOD\text{-}PDDA\text{-}CNTs\text{-}G)_3$-CNTs-G-SPCE.

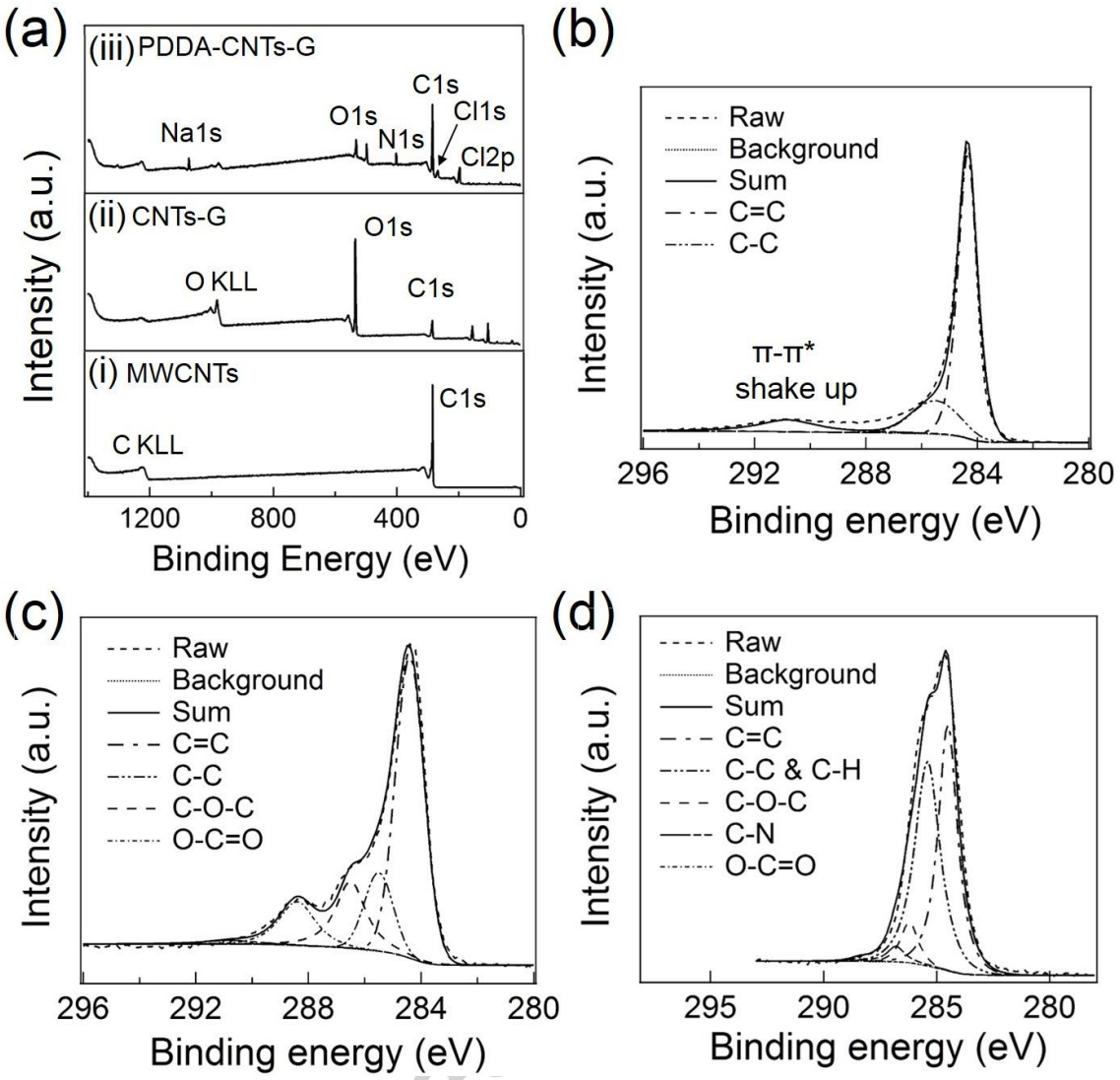

Fig. 2 (a) XPS survey spectra of (i) MWCNTs, (ii) CNTs-G, and (iii) PDDA-CNTs-G. Also, C1s XPS spectra of (b) MWCNTs, (c) CNTs-G, and (d) PDDA-CNTs-G.

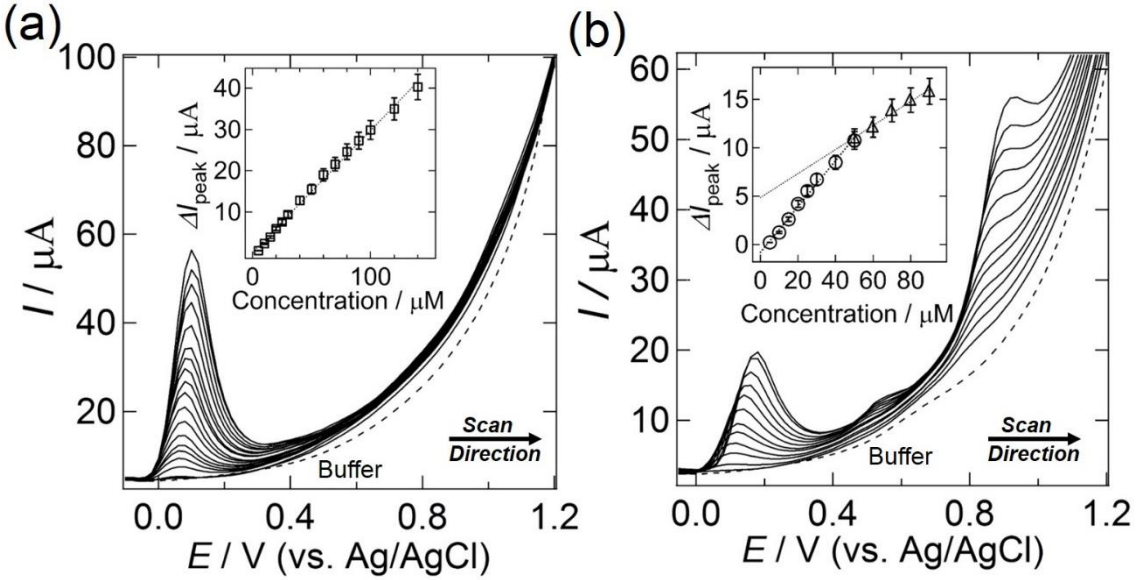

Fig. 3 (a) Representative SWV data for UA detection with the LbL biosensor composed of (XOD-PDDA-CNTs-G)$_3$-CNTs-G-SPCE and the inset is the plot of background corrected peak currents (ΔI_{peak}) versus different concentrations of UA. Concentrations were 5, 10, 15, 20, 25, 30, 35, 40, 50, 60, 70, 80, 90, 100, 120 and 140 μM. (b) A series of SWV data for Hx sensing using the LbL biosensor. The quantitation of Hx was achieved via measuring the oxidation peak current of UA produced by the catalytic reaction of Hx and XOD. The insert is the plot of peak currents versus Hx concentrations. Concentrations were 5, 10, 15, 20, 25, 30, 35, 40, 50, 60, 70, 80 and 90 μM.

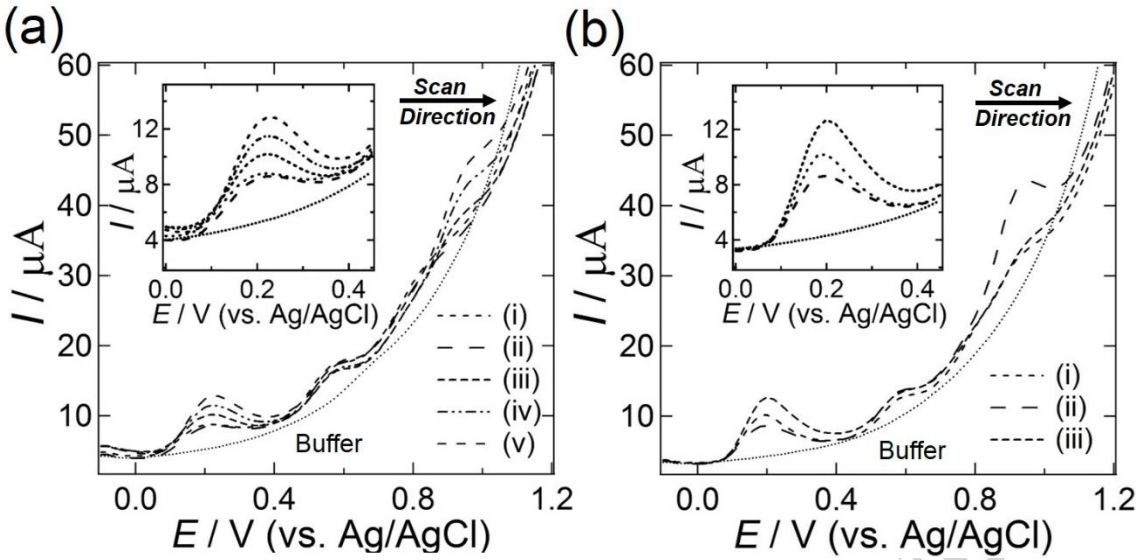

Fig. 4 Representative SWV data for the detection of Hx alongside spiking known concentrations of Hx in both 15-fold diluted normal human serum (a) and MI patient serum (b). Curve (i) in (a) and (b) was the signal from the diluted sample itself when using the LbL biosensor consisted of (XOD-PDDA-CNTs-G)$_3$-CNTs-G-SPCE while curve (iii), (iv), and (v) in (a) and (b) were the responses with the spiked Hx concentrations of 10, 15, and 20 μM, respectively. The peak response in (ii) in (a) and (b) was for the native UA present in the diluted serum samples obtained using the XOD free sensor composed of (PB-PDDA-CNTs-G)$_3$-CNTs-G-SPCE.

Tables

Table 1. Summary of Hx analysis for diluted normal human and MI patient serum solutions using our LbL sensor. The XOD free sensor was also used for evaluating the native UA concentration present in both serum samples. The data set for Hx analysis in both serum samples using an LC-MS method were compared for the validation of our LbL sensor performance.

Sample	C_{Hx}/μM (LbL biosensor)	Hx added /μM	Recovery (%)	RSD (%)	C_{Hx}/μM (LC-MS)
Normal serum (n=4)	9.11	10	91.05	4.77	0.08
	14.13	15	96.43	5.79	-
	20.37	20	101.86	5.52	-
MI patient serum (n=3)	8.77	0	-	5.31	8.78
	17.25	10	91.85	4.11	-

Dilution factor=15

Table 2. Summary of native UA concentration analysis for diluted normal human and MI patient serum solutions using XOD free sensor. Our results were also compared to those using an LC-MS method.

Sample NO.	C_{UA}/μM (Sensor)	RSD (%)	C_{UA}/μM (LC-MS)
Normal serum (n=4)	10.86	6.79	12.37
MI patient serum (n=3)	13.53	2.73	18.61

Dilution factor=15

Highlights

- A selective biosensor for hypoxanthine with a linear dynamic range of 5 to 50 μM
- Layer-by-layer assembly of carbon nanotubes/graphene complexes and xanthine oxidase
- Applications to normal human and myocardial infarction patient serum sample analyses
- Both uric acid and hypoxanthine can be simultaneously analyzed